JOURNAL OF THE PHYSICAL SOCIETY OF JAPAN, Vol. 49, No. 3, SEPTEMBER, 1980

Magnetic Excitations in a Metallic Antiferromagnet $FePt_3$

Masahumi KOHGI and Yoshikazu ISHIKAWA

Physics Department, Tohoku University, Sendai

(Received April 7, 1980)

Spin waves in an antiferromagnetic ordered alloy $FePt_3$ have been investigated in a wide range of temperature by means of neutron inelastic scattering techniques. From the dispersion relations of the spin waves at 5 K, the exchange interaction parameters between Fe atoms were determined based on the localized spin model, which were found to extend in long range with an oscillatory character. However, a renormalized spin wave theory with these parameters fails to reproduce the observed temperature dependence of the sublattice magnetization as well as the renormalization of the spin wave energy. This fact, together with the relatively large damping of the spin waves, suggests that the simple localized spin model is not sufficient to describe the spin dynamics in the alloy.

§1. Introduction

The alloy $FePt_3$ has a chemically ordered structure of Cu_3Au type with a lattice constant of $a=3.86$ A below about 1200 K.[1] It becomes antiferromagnetic below $T_N=170$ K with an antiferromagnetic wave vector of $\boldsymbol{Q}=2\pi/a(1/2, 1/2, 0)$, and only iron atoms carry a magnetic moment of 3.3 μ_B.[2] The magnetic structure is shown in Fig. 1(a). From these facts, $FePt_3$ is considered to be a particularly suitable material for detailed study of the spin dynamics in the metallic antiferromagnet. The relatively low Néel temperature and the large magnetic moment per atom offer a possibility of making measurements over wide range of temperatures and $\boldsymbol{q}$-space. The simple crystal and magnetic structures would be convenient for the analysis of the experimental results.

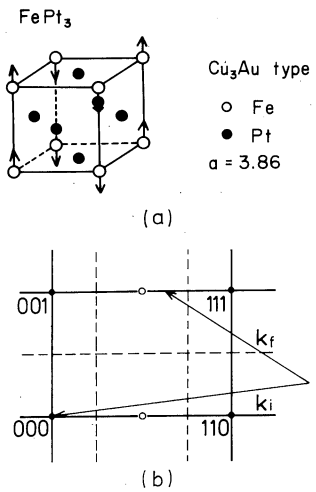

Fig. 1. (a) Crystal and magnetic structure of $FePt_3$. (b) $(1\bar{1}0)$ plane of the reciprocal lattice with zone boundaries of (1/2, 1/2, 0) domain (broken lines).

It is also pointed out that the spin dynamics in the iron group-platinum group alloys is expected to show the intermediate characteristics between the iron group metals and the localized spin systems like as Heusller alloys, since the high polarizability of 4*d* or 5*d* shells in these alloys is considered to play an important role on their magnetism. Recently, spin waves in the ferromagnetic alloy $FePd_3$, which is isomorphous with $FePt_3$, were investigated by means of neutron inelastic scattering techniques,[3] and it has been revealed that neither a localzed model nor a simple itinerant model are capable of providing a clear physical interpretation of the experimental results. Therefore, the investigation of spin dynamics in $FePt_3$ would give useful information as complementary one to understand the magnetism in these alloys from the side of the antiferromagnetism.

In this paper a neutron inelastic scattering study of the spin waves in $FePt_3$ at several temperatures below T_N is presented. The results at 5 K has already been reported briefly.[4] A study of the spin dynamics in $FePt_3$ above T_N will be discussed separately in another paper.[5]

§2. Experimental

2.1 *Sample*

The sample was a single crystal of 1.1 cm

in diameter and 3 cm long which was grown by Bridgman method after being prepared by melting the stoichiometric iron (99.99%) and platinum (99.9%) in an argon arc furnace. Chemical analysis showed the composition to be $Fe_{22.6}Pt_{77.4}$. The mosaic spread of the sample was estimated to be about 0.3° (FWHM) from rocking curves of neutron Bragg reflections. The antiferromagnetic structure of (1/2, 1/2, 0) type was confirmed by observing the 1/2, 1/2, 0 magnetic reflection below 170 K.

The 0, 0, 1/2 reflection was also found below about 80 K, whose intensity is about 1% of the 1/2, 1/2, 0 reflection at 5 K for an incident neutron energy of 55 meV. This indicates that a small amount of the (0, 0, 1/2) antiferromagnetic phase coexists below 80 K presumably due to slight deviation from the perfect atomic ordering.[2] We expect, however, that the (0, 0, 1/2) phase is too small to disturb the main phase. Really, no anoamly was observed near 80 K on the temperature dependence of the intensities of any magnetic reflection corresponding to the (1/2, 1/2, 0) antiferromagnetic phase. Therefore, we disregard it in our analysis.

The intensities of three different magnetic reflections 1/2, 1/2, 0; 1/2, 0, 1/2 and 0, 1/2, 1/2 were found to be nearly the same, suggesting that the three different antiferromagnetic domains would be equally distributed.

2.2 *Neutron scattering equipments*

The spin wave excitations at 5 K were measured with triple axis spectrometers IN1 at HFR, ILL and TUNS at JRR-2, JAERI. The spin wave excitations at higher temperatures as well as the temperature dependence of the sublattice magnetization were measured with TUNS. The monochromators were the copper (002) plane for IN1 and the pyrolytic graphite (002) plane for TUNS. The analyzers were pyrolytic graphite (002) plane for both of IN1 and TUNS. The horizontal and vertical collimations (FWHM) were 0.5°–1°–0.8°–1° and 0.5°–1°–1.5°–4°, respectively, for IN1 and 1°–0.5°–0.5°–1° and 1°–1.3°–2.4°–3°, respectively, for TUNS. The data were taken by fixing the incoming neutron energies at several selected values. The crystal was contained in a sealed aluminum can filled with helium exchange gas with a $[1\bar{1}0]$ axis vertical, which was attached to a copper tail-peace of a variable temperature cryostat. The sample temperatures were regulated to ± 0.1 K.

§3. Spin Waves at 5 K

3.1 *Experimental results*

The spin wave measurements were made mainly around the (1/2, 1/2, 0) and (1/2, 1/2, 1) reciprocal lattice points. The scattering plane is shown in Fig. 1(b), where the magnetic Brillouin zone boundaries corresponding to the (1/2, 1/2, 0) antiferromagnetic structure are plotted by broken lines. Well-defined magnon groups could be detected up to the magnetic zone boundaries in the principal axes [001], [110] and [111]. The dispersion relations obtained from the peak positions of the neutron groups are shown in Fig. 2. The wave vectors in the figure (and hereafter) are referred to the spin waves in the (1/2, 1/2, 0) domain. The symmetry of the scattering plane suggests that two spin wave branches should be observed; one from the (1/2, 1/2, 0) domain (*A* branch) and another from the (1/2, 0, 1/2) and the (0, 1/2, 1/2) domaines (*B* branch). Actually the neutron groups from both branches could be detected near the zone boundary of the [111] direction. However, the neutron groups near the zone center show only simple profiles with a single peak as displayed later in Fig. 3. In spite of the multidomain structure, the peak positions of them obey approximately an isotropic dispersion relation $\hbar\omega=\sqrt{c^2q^2+\Delta E^2}$ for $q\lesssim 0.16$ A^{-1} with $c=67$ meVA and $\Delta E=2$ meV.

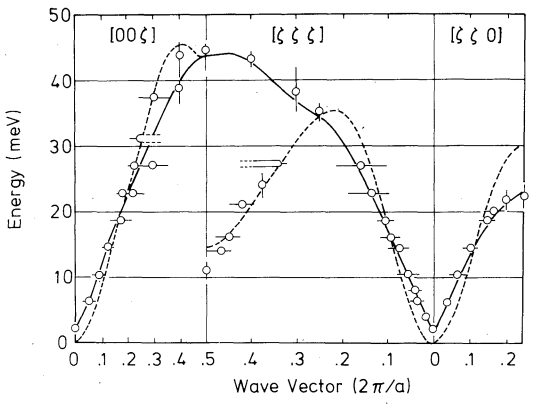

Fig. 2. Spin wave dispersion relations of $FePt_3$ at 5 K. The calculated dispersion curves based on the Heisenberg model (1) using six exchange parameters are shown by solid lines (*A* branch) and broken lines (*B* bransh).

3.2 Analysis by the localized spin model

The dispersion relations at 5 K were analyzed by the localized spin model. The Hamiltonian is described as

$$H=-2\sum_{\langle i,j\rangle} J_{ij}\boldsymbol{S}_i\boldsymbol{S}_j-D\sum_i S_{iz}^2, \qquad (1)$$

where J_{ij} is the effective exchange interaction between i-th and j-th iron atoms and D is the phenomenological anisotropy constant. The exchange interactions between iron and platinum atoms and those between platinum atoms are ignored because platinum atoms show no magnetic moment at the antiferromagnetic phase.[2)]

The dispersion relation of the antiferromagnetic spin wave is easily calculated in the free spin wave approximation as

$$\hbar\omega(\boldsymbol{q})=S\sqrt{A_0^2(\boldsymbol{q},\boldsymbol{Q})-B_0^2(\boldsymbol{q},\boldsymbol{Q})}, \qquad (2)$$

where

$$A_0(\boldsymbol{q},\boldsymbol{Q})=2J(\boldsymbol{Q})-J(\boldsymbol{q})-J(\boldsymbol{Q}+\boldsymbol{q})+2D,$$
$$B_0(\boldsymbol{q},\boldsymbol{Q})=J(\boldsymbol{q})-J(\boldsymbol{Q}+\boldsymbol{q}). \qquad (3)$$

Here S is the spin quantum number of the magnetic ion, $\boldsymbol{q}$ is the wave vector of the spin wave and $\boldsymbol{Q}$ is the antiferromagnetic wave vector: $\boldsymbol{Q}=2\pi/a(1/2, 1/2, 0)$ for $FePt_3$. $J(\boldsymbol{q})$ is the Fourier transform of the exchange interactions:

$$J(\boldsymbol{q})=\sum_{R_{ij}} J_{ij}\exp(i\boldsymbol{q}\boldsymbol{R}_{ij}).$$

Equation (2) was fitted to the measured spin wave dispersion relations at 5 K, using a nonlinear least squares procedure. Both A and B branches were taken into account in the calculation. In Table I are given the obtained exchange parameters for the different values of the number of the exchange parameters n. The anisotropy constant D was fixed in the least squares procedure to be $D=0.07$ meV which was determined so as to give the best fit at $\boldsymbol{q}=0$ in the case of $n=6$. S was assumed to be 3.3/2. The goodness of fit χ^2 is also listed in the table. For N measurements and n adjustable parameters, it is given by

$$\chi^2=(N-n)^{-1}\sum_{i=1}^{N}[(\hbar\omega_i^c-\hbar\omega_i)/\sigma_i]^2,$$

where $\hbar\omega_i^c$ and $\hbar\omega_i$ are the i-th calculated and measured spin wave energies and σ_i is the assigned error. Note that χ^2 decreases significantly with increasing n to 6, but it remains nearly constant with a further increase of n. Therefore it seems necessary to take account of the exchange interactions at least to sixth neighbors in order to fit the model (1) to the observations. The fitted spin wave dispersion curves using six exchange parameters are shown in Fig. 2 by solid curves for A branch and broken curves for B branch.

In Fig. 3(a) the exchange parameters for $n=8$ are shown as a function of the atomic distance. It is seen that the exchange interaction between iron atoms extends in long range and show an oscillatory character just as is the case with Heusller alloys.[6,7)] The Fourier transform $J(\boldsymbol{q})$ has its maximum at the wave vector $\boldsymbol{Q}=2\pi/a(1/2, 1/2, 0)$, as seen in Fig. 3(b). This confirms that these exchange parameters stabilize the antiferromagnetic structure of (1/2, 1/2, 0) type.

Some spin wave scattering profiles were calculated by folding the resolution function[8,9)]

Table I. Best fit exchange parameters between iron atoms in $FePt_3$ (units of meV).

n	2	4	6	8	10
J_1	−1.23±0.26	1.35±0.24	1.46±0.21	1.46±0.22	1.32±0.31
J_2	−1.14±0.28	−0.86±0.12	−0.82±0.13	−0.86±0.15	−0.73±0.20
J_3		0.66±0.05	0.70±0.07	0.72±0.08	0.73±0.07
J_4		0.41±0.05	0.27±0.07	0.27±0.07	0.27±0.07
J_5			0.05±0.05	0.07±0.07	0.05±0.08
J_6			−0.18±0.05	−0.21±0.06	−0.27±0.07
J_7				−0.03±0.04	−0.02±0.04
J_8				0.01±0.05	0.05±0.06
J_9					0.17±0.15
J_{10}					−0.02±0.07
χ^2	70.77	11.24	7.64	7.81	7.97

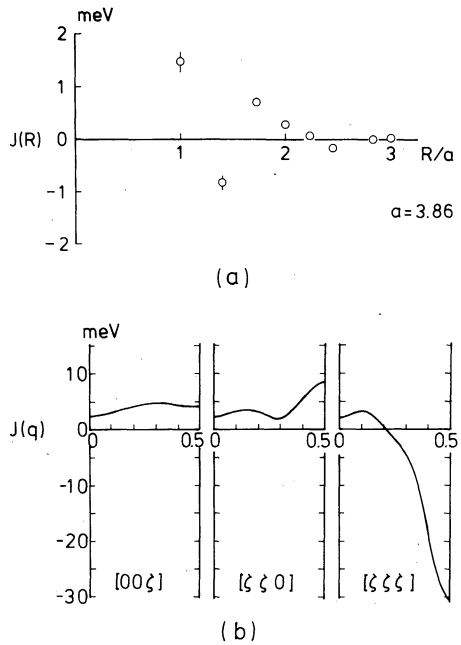

Fig. 3. (a) Exchange parameters between iron atoms in $FePt_3$ as a function of atomic distance. (b) Fourier transforms of the exchange parameters.

to the fitted dispersion curves by taking account of the structure factor for the spin wave scattering calculated also based on the model (1) and assuming the equal distribution of the domains. The calculated profiles of some constant-E scans are shown in Fig. 4 by broken lines and are compared with the observations. The contribution from each branch is indicated by arrows. It can be seen that the agreement betweem the calculations and the observations is satisfactory for the peak positions. Note that the peak positions of the calculated profiles for the lower energy scans are determined almost only by A branch. This is because the structure factor of A branch becomes much greater than that of B branch near the zone center, resulting in the apparent single peak profiles as observed experimentally. Therefore, it is concluded that the fitted dispersion relations agree generally well with the observations at least for the peak positions of the scattered neutrons. It is remarked, however, that most of the calculated profiles is narrower than the observed neutron groups as shown in Fig. 4. This point will be discussed in later sections.

§4. Temperature Dependence of Spin Wave Excitations

4.1 Experimental results

a. Sublattice magnetization

The temperature dependence of the sublattice magnetization was determined from that of the peak intensity of the 5/2, 5/2, 0 reflection obtained by using the incoming neutron energy of 55 meV. The non magnetic backgrounds estimated from the tails of the reflection were subtracted from the observed 5/2, 5/2, 0 intensities. The higher order contamination was found to be negligible. The obtained temperature dependence of the sublattice magnetization is shown in Fig. 5. The maximum error caused by extinction effect was estimated to be 5% at the lowest temperature from the comparison of the intensities of 1/2, 1/2, 0;

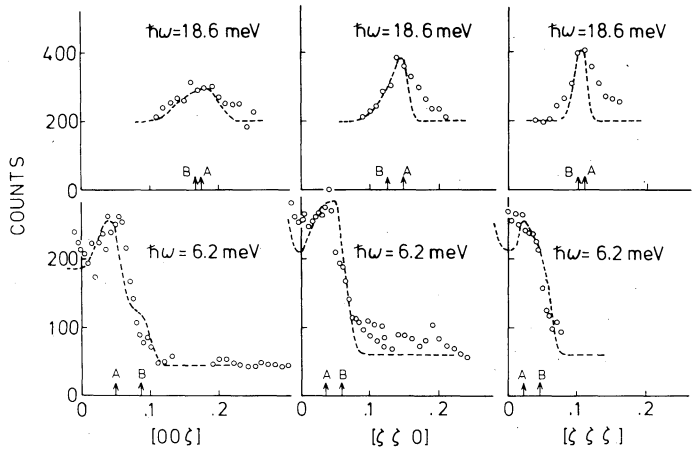

Fig. 4. Typical constant E scans at 5 K. The broken curves represent the calculated profiles obtained by convolution of the best fit dispersion relations with the resolution function. The arrows indicate the positions of each branch.

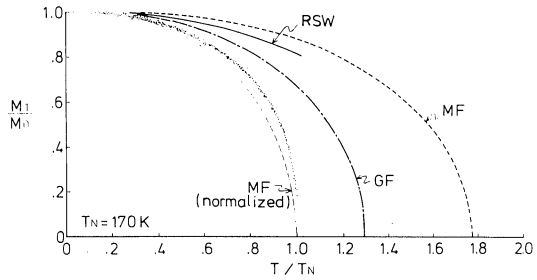

Fig. 5. Temperature dependence of the sublattice magnetization (dots) compared with the calculations based on the Heisenberg model (1) by the renormalized spin wave theory (RSW), the Green function method (GF) and the molecular field approximation (MF). The result of MF is also shown versus the normalized temperature to the calculated Néel temperature.

1/2, 1/2, 1; 3/2, 3/2, 0; 3/2, 3/2, 2 and 5/2, 5/2, 0 reflections at 77 K.

b. Spin waves

The spin wave excitations propagating in the [110] and the [111] directions were measured near the zone center at the temperatures of 80 K, 102 K, 127 K and 144.5 K (T/T_N=0.47, 0.6, 0.75 and 0.85, respectively). The constant-κ scans at (0.5, 0.5, 0) and (0.6, 0.6, 0) are shown in Fig. 6(a) and (b). The broken lines are the calculated lineshapes with infinite life time by using the dispersion relation (2) with six exchange parameters obtained at 5 K but changing the S value so as to fit the calculated peak positions to the observed ones. The solid lines in Fig. 6(b) show the least squares fit of the sum of two gaussians, that is, one for spin wave scattering and another for incoherent elastic scattering, to the observed neutron groups. It can be seen that the observed lineshapes are clearly broader than the calculated even at the low temperatures. The spin wave dispersion relations obtained from the peak positions of the observed neutron groups at the high temperatures are shown in Fig. 7 with the data at 5 K. Note that the gradient of the dispersion relation near the zone center decreases as the temperature raises. In Fig. 8 is displayed the observed renormalization of the spin wave excitations at $\boldsymbol{q}$=(0.1, 0.1, 0) and

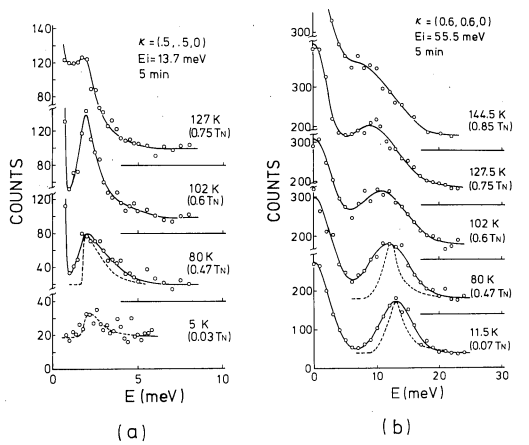

Fig. 6. Temperature dependence of the constant-κ scans with (a) κ=(0.5, 0.5, 0) and (b) κ=(0.6, 0.6, 0). The broken curves represent the calculated profiles obtained by convolution of the dispersion relations with the resolution functions. The solid lines in (b) show the least squares fit of two Gaussians to the experimental points.

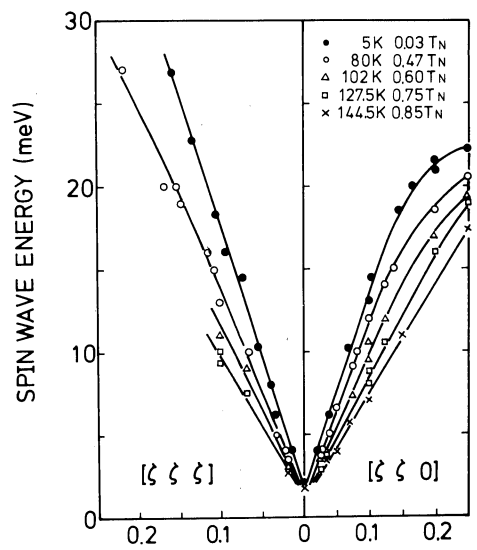

Fig. 7. Temperature dependence of the spin wave dispersion relations in the [110] and [111] axes.

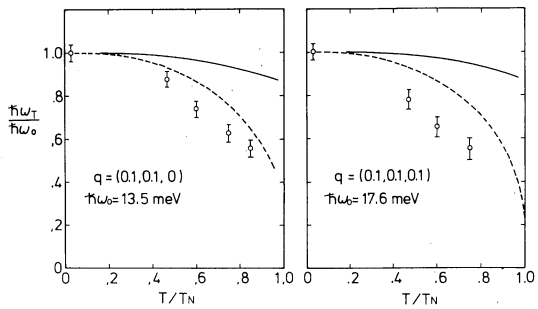

Fig. 8. Temperature dependence of the spin wave energies at $\boldsymbol{q}$=(0.1, 0.1, 0) and (0.1, 0.1, 0.1). The solid lines show the calculated by the renormalized spin wave theory. The broken lines show the sublattice magnetization.

(0.1, 0.1, 0.1). The temperature dependence of the sublattice magnetization is also shown by broken lines.

The line widths of the spin wave excitations were estimated approximately by using the equation $\Gamma=\sqrt{\Gamma_{ob}^2-\Gamma_i^2}$, where Γ_{ob} is the observed width and Γ_i is that of the instrumental resolution obtained from the calculation described above. The temperature dependence of the obtained width Γ (half width at half maximum) at $\boldsymbol{q}=(0.1, 0.1, 0)$ and $(0.1, 0.1, 0.1)$ are shown in Fig. 9. It can be seen that the width is anisotropic and does not vanish even at the lowest temperature.

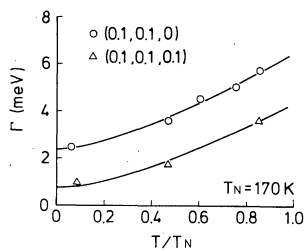

Fig. 9. Temperature dependence of the spin wave line widths (half width at half maximum) at $\boldsymbol{q}=$ (0.1, 0.1, 0) and (0.1, 0.1, 0).

4.2 *Comparison with the calculations based on the localized spin model*

The temperature dependence of spin wave energies and sublattice magnetization was compared with a calculation based on the Hamiltonian (1) using a renormalized spin wave theory (RSW), which treats the spin wave interaction terms by means of a random-phase approximation and determines self-consistently thermal averages of the magnon operator functions.[10,11] The exchange parameters to sixth neighbors determined at 5 K were used in the calculation. Self-consistent equations for the renormalized spin wave energy and the thermal averages of the magnon operators were solved at each temperature by using a successive approximation. Sums appeared in the equations which go over all wave vectors in the first Brillouin zone were replaced by those which go over 8×10^3 representative points. The calculation was iterated until spin wave energy converges within an errors of 0.1 meV.

The renormalized spin wave energies calculated at 5 K were found to differ slightly (about 1 meV in the largest case) from those of the free spin wave approximation. However, we did not try to change the values of the exchange parameters from the free spin wave results at 5 K in order to obtain better fit, because such a procedure is considered to affect little the temperature dependence of the spin wave energy and the sublattice magnetization in our analysis.

Temperature dependence of the sublattice magnetization based on the model (1) was also calculated by the molecular field approximation (MF) and the Green function method with the "Tyablicov" decoupling approximation (GF),[12] using the exchange parameters determined at 5 K and assuming $S=3/2$. Results of the RSW, the MF and the GF are shown by a solid line, a broken line and a chain-dashed line, respectively, in Fig. 5. The calculated curves fall off rapidly in the order of the GF, the RSW and the MF. In the case of the Heisenberg magnets, the GF is believed to give a little low transition temperatures,[13] and the RSW reproduces well the temperature dependence of the magnetization and the spin wave energy up to major part of the transition temperatures.[14-16] It can be seen, however, that the observed sublattice magnetization of $FePt_3$ falls off significantly fast even compared with that calculated by the GF.

The spin wave energies calculated by the RSW show also much weaker temperature dependence than the observations. Those at $\boldsymbol{q}=(0.1, 0.1, 0)$ and $(0.1, 0.1, 0.1)$ are shown by solid lines in Fig. 8. As seen in the figure, the calculated spin wave energies show only about 5% renormalization at $T=0.75\ T_N$, in strongly contrast with the observed 40% renormalization.

§5. Discussion

5.1 *Spin wave damping*

As described in §3 and 4, the experimental results show that there is rather large damping of spin waves in $FePt_3$. To discuss the origin of the damping, we compare it with that of some typical antiferromagnets, that is, $RbMnF_3$[17] as an example of the Heisenberg system, and $Mn_{73}Ni_{27}$[18] and $Fe_{70}Mn_{30}$[19] as those of the itinerant electron system. In order to make the comparison meaningful, we scaled

spin wave energies and line widths and temperatures by the spin wave energy $\hbar\omega_{ZB}$ at the zone boundary in the direction of the antiferromagnetic wave vector, following the way adopted for the analysis of spin wave damping in $RbMnF_3$.[17] In Fig. 10 are shown the reduced spin wave widths $\Gamma/\hbar\omega_{ZB}$ versus $\varepsilon^2\tau^3$ for $FePt_3$, $Mn_{73}Ni_{27}$, $Fe_{70}Mn_{30}$ and $RbMnF_3$, where ε and τ are the reduced spin wave energy and temperature defined as $\varepsilon=\hbar\omega_q/\hbar\omega_{ZB}$ and $\tau=2k_BT/\hbar\omega_{ZB}$, respectively. For $Mn_{73}Ni_{27}$ and $Fe_{70}Mn_{30}$, $\hbar\omega_{ZB}$ were roughly estimated to be 180 ± 30 meV and 150 ± 30 meV, respectively, extrapolating the reported data[18,19] to the zone boudaries and to 0 K, and only general trends of the reduced widths are shown by a broken line and a chain-dashed line, respectively. The results of $FePt_3$ and $RbMnF_3$ are shown in the figure by open circles and small closed circles, respectively. It was reported that the reduced width of $RbMnF_3$ is proportional to $\varepsilon^2\tau^3$ for $\tau\lesssim1$ as predicted by the theory[20] though the coefficient is greater by a factor of 6.[17]

Note that the trend of the reduced width of $FePt_3$ is much different from that of $RbMnF_3$; the magnitude of the reduced width of the former is much greater even near $\varepsilon^2\tau^3=0$ and increases with $\varepsilon^2\tau^3$ more rapidly than that of the latter. It is rather near to that of $Mn_{73}Ni_{27}$ and $Fe_{70}Mn_{30}$, though the slope seems not so steep as the latter cases. Since the substantial damping of spin waves observed for $Mn_{73}Ni_{27}$ and $Fe_{70}Mn_{30}$ is considered to be due to the interactions between single particle excitations

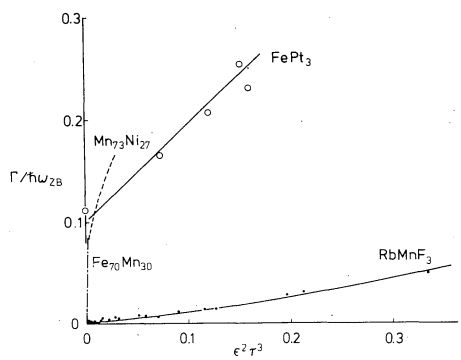

Fig. 10. Comparison of the reduced spin wave width $\Gamma/\hbar_Z\omega_B$ versus $\varepsilon^2\tau^3$ ($\varepsilon=\hbar\omega_q/\hbar\omega_{ZB}$ and $\tau=2k_BT/\hbar\omega_{ZB}$) for $FePt_3$ (open circles), $Mn_{73}Ni_{27}$ (broken line), $Fe_{70}Mn_{30}$ (chain-dashed line) and $RbMnF_3$ (small closed circles).

and spin wave modes in the itinerant 3*d*-electrons,[21,22] the above result may indicate that the damping of spin waves in $FePt_3$ is also attributed, at least in part, to the same origin, though in $FePt_3$ the contribution of 5*d*-electrons may be important.

It is also emphasized that the characteristic of the spin wave damping of $FePt_3$ contrasts with that of the isomorphous ferromagnetic alloy $FePd_3$. In the case of $FePt_3$ the relatively large damping of spin wave exists at wide range of wave vectors, even near zone center; while in the case of $FePd_3$ the substantial damping of spin waves develops beyond some definite values of wave vectors (beyond the energies of about 40 meV).[3] The difference of the characteristics of the spin wave damping between them is just what is expected in the itinerant electron systems.[25] This fact also supports the itinerant electron origin of the spin wave damping in these alloys.

5.2 *Conclusive remarks*

In §4 it has been revealed that the localized spin model (1), which was successful for interpreting the spin wave dispersion at the low temperature, could not reproduce well the temperature dependence of the spin wave energies as well as the sublattice magnetization of $FePt_3$. The existence of the relatively large damping of spin waves also suggests the insufficiency of the simple model. One explanation of the descrepancy between the model and the observation is described below.

In the model (1) the role of the 5*d* electrons of platinum atoms in the spin dynamics of $FePt_3$ was assumed to be just like as that of the *s*-electrons in the so-called *s-d* interaction system for which the adiavatic approximation is valid. It is well known, however, that platinum atoms are easily polarized to carry magnetic moment of the order of 0.1 to 1 μ_B in the ferromagnetic alloys with the iron-group elements. In fact, in $MnPt_3$ and $CoPt_3$, which are isomorphous with $FePt_3$ but ferromagnetic, platinum atoms have magnetic moment of 0.26 μ_B at 77 K for both cases.[23,24] Therefore it is reasonably said that the absence of detectable moment on platinum atoms in $FePt_3$ is only due to its magnetic structure which cancels the exchange field by the iron moments at the platinum atom sites, and the

existence of the high polarizability of the 5*d* electrons may result in additional effects on the spin dynamics which were neglected in the model.

One of them would be the direct effect of the polarization of the platinum atoms caused by the deviation from the cancellation of the exchange field by spin wave modes or by external field. In the antiferromagnetic state, spin waves on the iron lattice may be accompanied with the local polarization of 5*d* electrons on platinum atoms because of the local breakdown of the cancellation of the exchange field. This would contribute to a rapid decrease of the observed sublattice magnetization more than that expected by the calculation based on the model (1).

The paramagnetic scattering experiments for $FePt_3$, details of which will be discussed in another paper,[5] have revealed that the magnetic moment per iron atom calculated from the "Curie-Weiss constant" of the staggered susceptibility $\chi(\boldsymbol{Q})$ was nearly same as the value observed at 4.2 K,[2] but that calculated from the uniform susceptibility $\chi(0)$ was about twice of the low temperature value, that is, $4\,\mu_B$ from $\chi(\boldsymbol{Q})$ and $5.7\,\mu_B$ from $\chi(0)$. This phenomena would also be interpreted in terms of the polarization of the platinum atoms; under the staggered field ($\boldsymbol{\kappa}=\boldsymbol{Q}$) the polarization of the platinum atoms may be negligible because of the cancellation of the exchange field: but, under the uniform field ($\boldsymbol{\kappa}=0$), $\chi(0)$ would be enhanced because of the polarization of platinum atoms by the nonzero exchange field from the iron lattice.

The high polarizability of the 5*d*-electrons of platinum atoms would also cause the temperature dependence of the exchange parameters between iron atoms. This is because the electronic structure of the 5*d*-electrons, to which the magnitude of the exchange parameters is sensitive, would be strongly dependent on the magnetic structure or even on the degree of the magnetic ordering on account of the high polarizability. The rapid decrease of the spin wave excitation energies and the fairly low Néel temperature compared with the calculations based on the model (1) probably come from this effect.

If the effects of the polarization of the 5*d*-electrons of platinum atoms on the spin dynamics are so strong as described above, the interactions between spin wave modes and single particle excitations in the itinerant 5*d*-electrons would not be negligible. As in the itinerant electron antiferromagnet such interactions give rise to large spin wave damping, nearly the same situation is also expected in our system. This would result in the large spin wave damping of $FePt_3$ similar to that of the typical itinerant antiferromagnet as described in the beginning of this section.

Though the above explanation for the spin dynamics of $FePt_3$ is only in the stage of a conjecture, such an approach would be quite fruitful for understanding the spin dynamics in the systems like as the iron group-platinum group alloys. We hope that our results promote further theoretical studies on this kind of materials. The band theoretical calculation would be particulaly of importance.

Acknowledgements

A part of this work was supported by the Institut Laue-Langevin and also by Japan-France Scientific Cooperation Program sponsored by the Japan Society for Promotion of Science and Centre National de la Recherche Scientifique. The authors especially wish to thank Dr. P. Radhakrishna for his helpful cooperation and Dr. J. Copley for his kind assistance during the experiments at ILL. One of the authors (M. K.) thanks Professor D. Bloch for patial support in his stay at Laboratoire de Magnetisme. The authors also wish to acknowledge the useful discussions with their colleagues, Y. Endoh and K. Tajima, and the technical help of M. Onodera, M. Suzuki and K. Nemoto. Numerical calculations were carried out in the Computer Center of Tohoku University.

References

1) J. Crangle and J. A. Shaw: Phil. Mag. **7** (1962) 207.
2) G. E. Bacon and J. Crangle: Proc. R. Soc. London A **272** (1963) 387.
3) A. J. Smith, W. G. Stirling and T. H. Holden: J. Phys. F (Metal Phys.) **7** (1977) 2411, and references therein.
4) M. Kohgi, Y. Ishikawa and P. Radhakrishna: Solid State Commun. **27** (1978) 409.
5) M. Kohgi and Y. Ishikawa: J. Phys. Soc. Jpn. **49** (1980) 994.
6) Y. Noda and Y. Ishikawa: J. Phys. Soc. Jpn.

40 (1976) 690.
7) K. Tajima, Y. Ishikawa, P. J. Webster, M. W. Stringfellow, D. Tocchetti and K. R. A. Zeabeck: J. Phys. Soc. Jpn. **43** (1977) 483.
8) M. J. Cooper and R. Nathans: Acta Cryst. **23** (1967) 357.
9) N. J. Chesser and J. D. Axe: Acta Cryst. **A29** (1973) 160.
10) O. Nagai: Phys. Rev. **180** (1969) 557.
11) I. Harada and K. Motizuki: J. Phys. Soc. Jpn. **32** (1972) 927.
12) M. E. Lines: Phys. Rev. **135** (1964) A1336.
13) M. E. Lines and E. D. Jones: Phys. Rev. **139** (1965) A1313.
14) G. G. Low: *Proceedings of the Chalk River Symposium on Inelastic Scattering of Neutrons* (IAEA, Vienna, 1965) p. 453.
15) M. Kohgi, Y. Ishikawa, I. Harada and K. Motizuki: J. Phys. Soc. Jpn. **36** (1974) 112.
16) V. K. Tondon and M. F. Collins: Int. J. Magnetism **6** (1974) 283.
17) C. G. Windsor, D. H. Saunderson and E. Schedler: Phys. Rev. Lett. **37** (1976) 855.
18) B. Hennion, M. T. Hutchings, R. D. Lowde, M. W. Stringfellow and D. Tocchetti: *Proc. Conf. Neutron Scattering, Gatlinburg, 1976.*
19) K. Tajima, Y. Ishikawa and Y. Endoh: J. Phys. Soc. Jpn. **41** (1976) 1195.
20) A. B. Harris, D. Kumar, B. I. Halperin and P. C. Hohenberg: Phys. Rev. **B3** (1971) 961.
21) M. J. Gillan: J. Phys. F; Metal Phys. **3** (1973) 1874.
22) W. Young: Physica **91B** (1977) 213.
23) B. Antonini, F. Lucari, F. Menzinger and A. Paoletti: Phys. Rev. **187** (1969) 611.
24) F. Menzinger and A. Paoletti: Phys. Rev. **143** (1966) 365.
25) Y. Ishikawa: J. Appl. Phys. **49** (1978) 2125.